

Multi-quasiparticle γ -band structure in neutron-deficient Ce and Nd isotopes

J.A. Sheikh^{1,2,3}, G.H. Bhat³, R. Palit⁴, Z. Naik⁴, Y. Sun^{2,5,6}

¹*Physics Division, Oak Ridge National Laboratory, P.O. Box 2008, Oak Ridge, Tennessee 37831, USA*

²*Department of Physics and Astronomy, University of Tennessee, Knoxville, Tennessee 37996, USA*

³*Department of Physics, University of Kashmir, Srinagar, 190 006, India*

⁴*Tata Institute of Fundamental Research, Colaba, Mumbai, 400 005, India*

⁵*Department of Physics, Shanghai Jiao Tong University, Shanghai 200240, P. R. China*

⁶*Institute of Modern Physics, Chinese Academy of Sciences, Lanzhou 730000, P. R. China*

Abstract

The newly developed multi-quasiparticle triaxial projected shell-model approach is employed to study the high-spin band structures in neutron-deficient even-even Ce- and Nd-isotopes. It is observed that γ -bands are built on each intrinsic configuration of the triaxial mean-field deformation. Due to the fact that a triaxial configuration is a superposition of several K -states, the projection from these states results in several low-lying bands originating from the same intrinsic configuration. This generalizes the well-known concept of the surface γ -oscillation in deformed nuclei based on the ground-state to γ -bands built on multi-quasiparticle configurations. This new feature provides an alternative explanation on the observation of two $I = 10$ aligning states in ^{134}Ce and both exhibiting a neutron character.

Key words: triaxial deformation, γ -vibration, two-quasiparticle states, triaxial projected shell model

PACS: 21.60.Cs, 21.10.Re, 27.60.+j

1 Introduction

One of the main challenges in nuclear structure is to understand the interplay between single-particle, vibrational and rotational degrees of excitation modes. Mass $A = 120 - 130$ is one of the regions where the modes associated with all three degrees of freedom have been studied quite extensively.

High-spin band structure in this mass region has been experimentally investigated through heavy-ion-induced reactions (see, for example, refs. [1,2,3,4,5]). Along with these studies, many low-lying non-yrast states have also been investigated in the β -decay spectroscopic methods [6] and Coulomb excitations of stable as well as radioactive ions [7,8,9]. Nuclei in this mass region depict a variety of band structures which are built on different excitation modes. Proton and neutron mass distributions develop opposite types of quadrupole deformations in these nuclei due to the presence of the proton Fermi surface near the lower end of the $h_{11/2}$ orbitals and that of neutron near the middle of the $h_{11/2}$ orbitals. This results in a γ -instability in these nuclei, and the γ -soft behavior is manifested in the observed low-lying quasi- γ bands. This region thus provides an excellent opportunity to study the effect of rotation and quasiparticle excitation on the top of γ -vibrations.

As the aligning neutrons and protons in these rotating systems are occupying the same intruder orbit $1h_{11/2}$, the neutron and proton quasiparticle (qp) alignment processes compete in this mass region. In the majority of the nuclei in this mass region, the proton alignment occurs earlier than the neutron alignment, which is well described in the Woods-Saxon TRS framework [10,11]. However, the neutron alignment is observed to be delayed in many cases, and the Woods-Saxon TRS analysis always under-predicts this rotational alignment. There have been other intriguing observations in this mass region. One problem is in the g-factor measurement in ^{134}Ce for the lowest two $I = 10$ states, which lie very close to each other. The issue is that both of these states are shown to have a neutron character [12] and since these $I = 10$ states are considered to be the bandheads of 2-qp bands, two 2-quasineutron band structures are observed in ^{134}Ce . This is quite surprising as normally lowest-lying two 2-qp states should belong to 2-quasineutron and 2-quasiproton states.

Thus, with the collective and quasiparticle excitations coexisting in the complex low-lying spectrum in these γ -soft nuclei, it is desirable to have a microscopic method that can handle all these degrees of freedom self-consistently. The early version [13] of the triaxial projected shell model (TPSM) adopted the triaxially deformed qp vacuum configuration and performed three-dimensional angular momentum projection. It was shown [14] that one can use this simple configuration to produce collective multi-phonon γ -vibrational bands at low spin states. In this earlier version, mixing with quasiparticle excitations was neglected and, therefore, it cannot describe excitation of quasiparticles in a triaxially deformed mean field. This limitation has been relaxed in our recent development [15] and the TPSM quasiparticle space for even-even systems has been considerably extended by inclusion of many 2- and 4-qp configurations. In a parallel work, a similar extension was done for odd-odd nuclei [16]. These new developments provide a suitable shell-model framework to investigate, microscopically, the current topical issues in nuclear structure that are related to triaxiality, such as the problem of γ -bands built on multi-quasiparticle con-

figurations, discussed in the present work. They are also applicable to the problems related to the wobbling motion and to the so-called chiral doublet band structures, which will be the focus of our future investigations.

The purpose of the present work is to demonstrate that the traditional picture of γ -vibration in deformed nuclei, based on the ground-state configuration, can be generalized to the case of multi-qp configurations. In the TPSM description, projected states with $K = 0, 2$, and 4 from the 0-qp configuration correspond to ground, γ -, and 2γ - bands [14]. Similar to these γ - and 2γ - bands built on the ground state, new multi-phonon γ -bands are based on multi-qp states. For the multi-qp bands, projection with different K -values will correspond to qp-excited γ -bands. In particular, we shall show that the projected $K = 1$ and 3 configurations originating from the same intrinsic neutron 2-qp configuration correspond to the two $I = 10$ states observed in ^{134}Ce . This provides a plausible explanation to the early observation of the $I = 10$ states in this nucleus with similar intrinsic structure.

The paper is organized as follows: In Section 2, we outline some basic elements of the TPSM approach. For more details about TPSM, we refer the reader to ref. [15] and references cited therein. In Section 3, calculations and discussions on neutron-deficient Ce and Nd isotopes are presented. Finally in Section 4, we summarize the present work.

2 Outline of the Theory

The extended TPSM qp basis [15] consists of (angular-momentum) projected qp vacuum (0-qp state), two-proton ($2p$), two-neutron ($2n$), and 4-qp states, i.e.,

$$\{\hat{P}_{MK}^I |\Phi\rangle, \hat{P}_{MK}^I a_{p_1}^\dagger a_{p_2}^\dagger |\Phi\rangle, \hat{P}_{MK}^I a_{n_1}^\dagger a_{n_2}^\dagger |\Phi\rangle, \hat{P}_{MK}^I a_{p_1}^\dagger a_{p_2}^\dagger a_{n_1}^\dagger a_{n_2}^\dagger |\Phi\rangle\}, \quad (1)$$

where the three-dimensional angular-momentum-projection operator is

$$\hat{P}_{MK}^I = \frac{2I+1}{8\pi^2} \int d\Omega D_{MK}^I(\Omega) \hat{R}(\Omega), \quad (2)$$

with the rotation operator $\hat{R}(\Omega) = e^{-i\alpha\hat{J}_z} e^{-i\beta\hat{J}_y} e^{-i\gamma\hat{J}_z}$. $|\Phi\rangle$ in (1) is the triaxially-deformed qp vacuum state. The qp basis chosen above is adequate to describe high-spin states up to $I \sim 20\hbar$ for nuclei considered in this work. In the present analysis we shall, therefore, restrict our discussion to this spin regime.

It is important to note that for the case of axial symmetry, the qp vacuum state has $K = 0$ [17], whereas in the present case of triaxial deformation, the

vacuum state is a superposition of all possible K -values. Rotational bands with the triaxial basis states, Eq. (1), are obtained by specifying different values for the K -quantum number in the angular-momentum projector in Eq. (2). The allowed values of the K -quantum number for a given intrinsic state are obtained through the following symmetry consideration. For $\hat{S} = e^{-i\pi\hat{J}_z}$, we have

$$\hat{P}_{MK}^I |\Phi\rangle = \hat{P}_{MK}^I \hat{S}^\dagger \hat{S} |\Phi\rangle = e^{i\pi(K-\kappa)} \hat{P}_{MK}^I |\Phi\rangle, \quad (3)$$

where $\hat{S} |\Phi\rangle = e^{-i\pi\kappa} |\Phi\rangle$. For the self-conjugate vacuum or 0-qp state, $\kappa = 0$ and, therefore, it follows from the above equation that only $K = \text{even}$ values are permitted for this state. For 2-qp states, $a^\dagger a^\dagger |\Phi\rangle$, the possible values for K -quantum number are both even and odd, depending on the structure of the qp state. For example, for a 2-qp state formed from the combination of the normal and the time-reversed states $\kappa = 0$, only $K = \text{even}$ values are permitted. For the combination of the two normal states, $\kappa = 1$ and only $K = \text{odd}$ states are permitted.

As in the earlier projected shell-model calculations, we use the pairing plus quadrupole-quadrupole Hamiltonian [17], with a quadrupole-pairing term also included:

$$\hat{H} = \hat{H}_0 - \frac{1}{2}\chi \sum_{\mu} \hat{Q}_{\mu}^{\dagger} \hat{Q}_{\mu} - G_M \hat{P}^{\dagger} \hat{P} - G_Q \sum_{\mu} \hat{P}_{\mu}^{\dagger} \hat{P}_{\mu}. \quad (4)$$

It has been shown by Dufour and Zuker [18] that these interaction terms simulate the essence of the important correlations in nuclei and even the realistic force has to contain, at least, these basic components implicitly in order to work successfully in the structure calculations. Some large-scale spherical shell-model calculations [19] also adopt this type of interaction.

The triaxially deformed single-particle basis is obtained from the Nilsson model [20]. The corresponding triaxial Nilsson mean-field Hamiltonian is given by

$$\hat{H}_N = \hat{H}_0 - \frac{2}{3}\hbar\omega \left\{ \epsilon \hat{Q}_0 + \epsilon' \frac{\hat{Q}_{+2} + \hat{Q}_{-2}}{\sqrt{2}} \right\}, \quad (5)$$

in which ϵ and ϵ' specify the axial and triaxial deformation, respectively. ϵ and ϵ' are related to the conventional triaxiality parameter by $\gamma = \tan^{-1}(\epsilon'/\epsilon)$. In (5), \hat{H}_0 is the spherical single-particle Hamiltonian, which contains a proper spin-orbit force [20]. The interaction strengths in (4) are taken as follows: the QQ -force strength χ is adjusted such that the physical quadrupole deformation

Table 1

Axial and triaxial quadrupole deformation parameters ϵ and ϵ' employed in the TPSM calculation for $^{128-134}\text{Ce}$ and $^{132-138}\text{Nd}$ isotopes. The corresponding conventional triaxiality parameter γ (in degree) is also given.

Ce nuclei	ϵ	ϵ'	γ	Nd nuclei	ϵ	ϵ'	γ
^{128}Ce	0.250	0.120	26	^{132}Nd	0.267	0.120	24
^{130}Ce	0.225	0.120	28	^{134}Nd	0.200	0.120	31
^{132}Ce	0.183	0.100	29	^{136}Nd	0.158	0.110	35
^{134}Ce	0.150	0.100	34	^{138}Nd	0.170	0.110	33

ϵ is obtained as a result of the self-consistent mean-field HFB calculation [17]. The monopole pairing strength G_M is of the standard form

$$G_M = \frac{G_1 - G_2 \frac{N-Z}{A}}{A} \text{ for neutrons, } G_M = \frac{G_1}{A} \text{ for protons.} \quad (6)$$

In the present calculation, we take $G_1 = 20.82$ and $G_2 = 13.58$, which approximately reproduce the observed odd-even mass difference in the mass region. This choice of G_M is appropriate for the single-particle space employed in the model, where three major shells are used for each type of nucleons ($N = 3, 4, 5$ for both neutrons and protons). The quadrupole pairing strength G_Q is assumed to be proportional to G_M , and the proportionality constant being fixed as 0.18.

3 Results and Discussion

TPSM calculations have been performed for four even-even isotopic chains of $^{128-134}\text{Ce}$ and $^{132-138}\text{Nd}$ nuclei. As already mentioned in the introduction, the main emphasis of the present work is to perform a detailed investigation of the yrast- and γ -bands beyond the first band crossing. The above-mentioned nuclei were chosen as they have well-developed γ -bands observed experimentally and for some of them up to high spins. The input parameters in the calculation are the deformation parameters ϵ and ϵ' , which are given in Table 1. The corresponding conventional triaxiality parameter γ (in degree) is also given. The quadrupole deformation ϵ in the table are those of Möller and Nix [21] (with exception for ^{138}Nd , see discussion below) and the triaxiality parameter ϵ' have been calculated from the projected potential energy surface. In Fig. 1, we provide one example from such calculations, in which projected energies as functions of ϵ' for a fixed ϵ ($\epsilon = 0.2$ in the ^{134}Nd case) are plotted for the low spin states. In this figure, the γ -soft nature of the nucleus is clearly seen since the curves are all flat with triaxiality, specially for $\epsilon' > 0.08$. As shown in

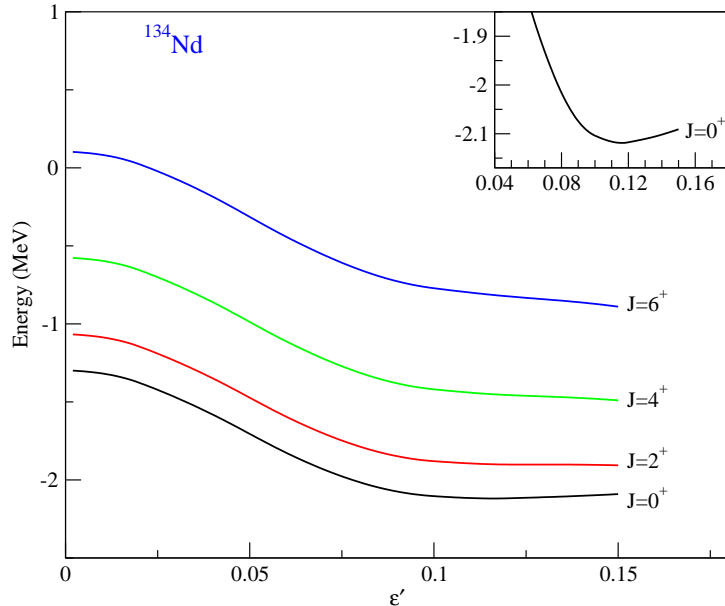


Fig. 1. (Color online) Calculated projected energy-surfaces for the low spin states in ^{134}Nd .

the inset in Fig. 1, a minimum in the projected ground-state energy is present at $\epsilon' \approx 0.12$. Thus, projected ground-state energies have been calculated for a range of ϵ' values, and the value which gives rise to the minimum energy is used in all further TPSM calculations. We would like to mention that in one of the studied nuclei, ^{138}Nd , ref. [21] predicted a negative value of ϵ corresponding to an oblate deformation in its ground state, which is in disagreement with all other neighboring nuclei. However, the TRS calculation [22] for this nucleus indicates a large triaxiality of $\gamma \approx 30^\circ$. In our calculation, we therefore take a positive ϵ with a sizable ϵ' to construct the basis.

The calculations are performed in two stages. In the first step, the projected states are obtained from the triaxially deformed qp states by applying the three-dimensional angular-momentum projection method. The projection is carried out for configurations constructed from various intrinsic states close to the Fermi surface. We have performed the angular-momentum projection for all the qp configurations, which are built by considering the single-particle states that are within 3 MeV from the Fermi surfaces. In the second stage, the shell-model Hamiltonian, Eq. (4), is diagonalized with the projected states as the basis configurations.

The lowest three bands obtained after diagonalization for each angular momentum are shown in Fig. 2 for all the studied Ce and Nd isotopes. These bands have the main component from the 0-qp state and, therefore, are collective bands in the low-spin regime. Theoretical $K = 0$ and $K = 2$ bands are respectively compared to the data of the yrast and γ -vibrational (one-phonon) bands, and the $K = 4$ bands are our prediction for possible 2γ (two-phonon)

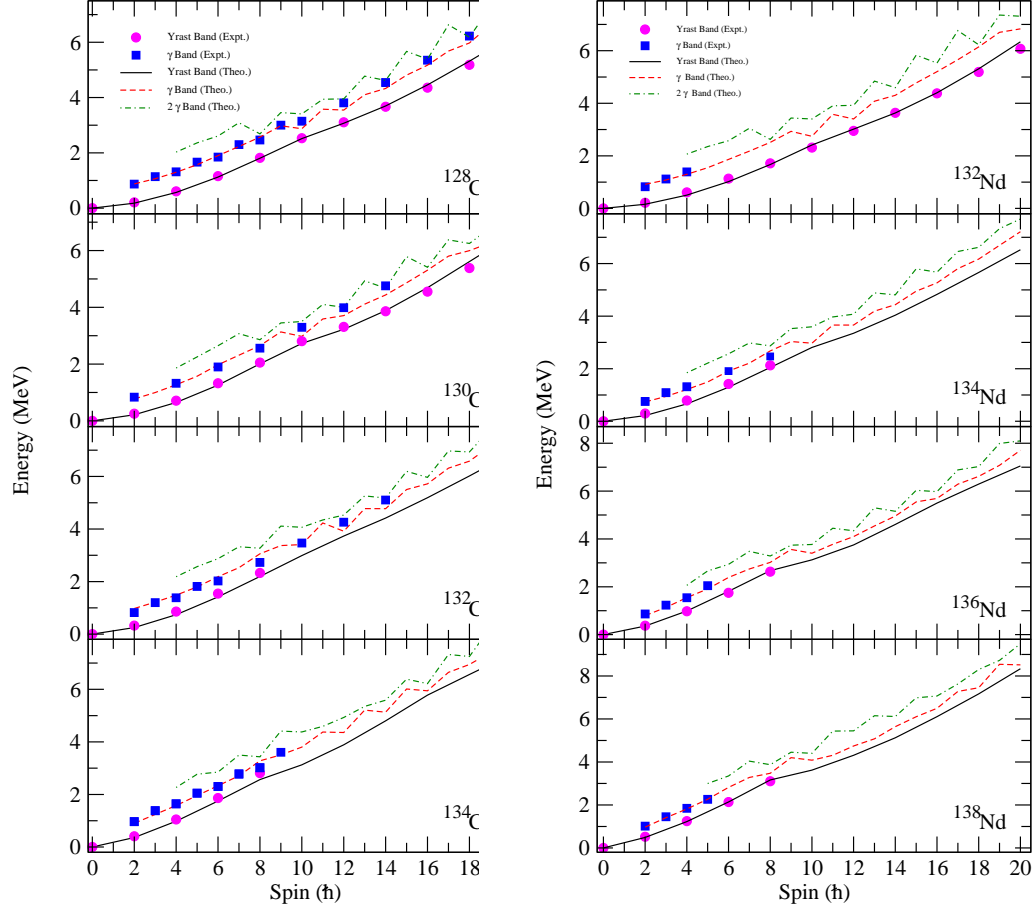


Fig. 2. (Color online) Comparison of experimental and calculated band structures for $^{128-134}\text{Ce}$ and $^{132-138}\text{Nd}$. Data are taken from ref. [23] (^{128}Ce), [24] (^{130}Ce), [1] (^{132}Ce), [25] (^{134}Ce), [26] (^{132}Nd), [27] (^{134}Nd), [28] (^{136}Nd), and [29] (^{138}Nd).

bands. It can be seen that, overall, an excellent reproduction for the known data has been achieved. In particular, the experimental γ -band in ^{128}Ce is well reproduced up to the highest spin state studied in this work. The calculated γ -band in $^{136,138}\text{Nd}$ is predicted to lie very close in energy to the yrast band, in agreement with known data, and the two bands become nearly degenerate at high spins.

It is clearly noted in Fig. 2 that yrast bands for all studied isotopes have two slopes, corresponding to crossings of bands with two distinct configurations. The change in slope occurs at spin $I = 8$ or 10 . This feature has been well described by the calculation, for the isotopes $^{128,130}\text{Ce}$ and ^{132}Nd where high-spin data exist. Furthermore, we observe that for the rest of nuclei, i.e., $^{132,134}\text{Ce}$ and $^{134,136,138}\text{Nd}$, the current ground-band data are available only before the predicted onset of the band-crossing at $I = 10$. The first and second excited bands at low-spins are predominantly composed of the collective γ and 2γ structures, but the high-spin states of these bands have considerable mixing with the 2-qp states. The calculation also predicts some energy staggerings in

the γ - and 2γ - bands. The staggering divides a rotational band with $\Delta I = 1$ into two branches with $\Delta I = 2$. In the isotopes $^{128,130,132}\text{Ce}$ where high-spin data of the γ -band are known, we see that the experimental bands actually belong to one of the branches of the staggering γ -bands, namely the energetically favored one with even spins. The present calculation further predicts some irregularities in the staggering of γ - and 2γ - bands due to band mixing (e.g. staggering appears in a certain spin range but diminishes at high spins). We hope that our results can serve as a guidance for future experiments to identify γ - and 2γ - bands in this mass region.

To extract structure information from the calculation, it is useful to discuss the energies in terms of band diagrams [17]. A band diagram is an ensemble of projected band energies for intrinsic configurations, i.e., the diagonal matrix elements before band mixing. It usually shows crossings of various bands where some prominent phenomena may take place, and therefore plays a central role in the interpretation of numerical results. One must keep track of the configurations of each band when plotting a band diagram. As already mentioned, with the triaxial basis, the intrinsic states do not have a well-defined K quantum number. Each triaxial configuration in (1) is a composition of several K values, and bands in band diagrams are obtained by assigning a given K value in the projection operator. As in ref. [15], we denote a K state of an i configuration as (K, i) , with $i = 0, 2n, 2p$, and 4. For example, $K = 0$ state of the 0-qp configuration is marked as $(0, 0)$ and $K = 1$ of the $2n$ -qp configuration as $(1, 2n)$.

Band diagrams of the studied cerium isotopes from $A = 128$ to 134 are presented in Fig. 3. For $^{128,130}\text{Ce}$, the $(2, 0)$ bandhead energy is approximately 0.8 MeV and the $(4, 0)$ bandhead is slightly below 2 MeV. Further, in both nuclei, the $2p$ bandhead is slightly at a lower excitation energy than the $2n$ bandhead, and due to this difference, the $2p$ band crosses the ground band earlier than the $2n$ band. The $2p$ band, $(1, 2p)$ crosses the ground band $(0, 0)$ in both nuclei at $I = 10$ and the proton structure of the first crossing is validated by the systematics of the band-crossings [30]. The g-factor measurement has been done for the $I = 10^+$ state of ^{126}Ce and has a very large value of 1.0, therefore indicating that the first band-crossing is indeed due to the alignment of protons for this nucleus. From the known experimental result and from the systematics of the proton crossing as a function of mass number, it was concluded in ref. [30] that $^{128-132}\text{Ce}$ have proton crossing occurring first.

The band diagrams in Fig. 3 depict $(2, 0)$ and $(4, 0)$ bandheads for $^{132,134}\text{Ce}$ at a similar excitation energy as that of lighter Ce-isotopes. However, it is noted that the $2n$ bandhead is lower than the $2p$ bandheads as compared to the $^{128,130}\text{Ce}$ isotopes. Due to this lowering of the neutron 2-qp band, the band-crossing features in the two pictures on the right column in Fig. 3 are qualitatively different from those of the left column. In ^{132}Ce , it is observed

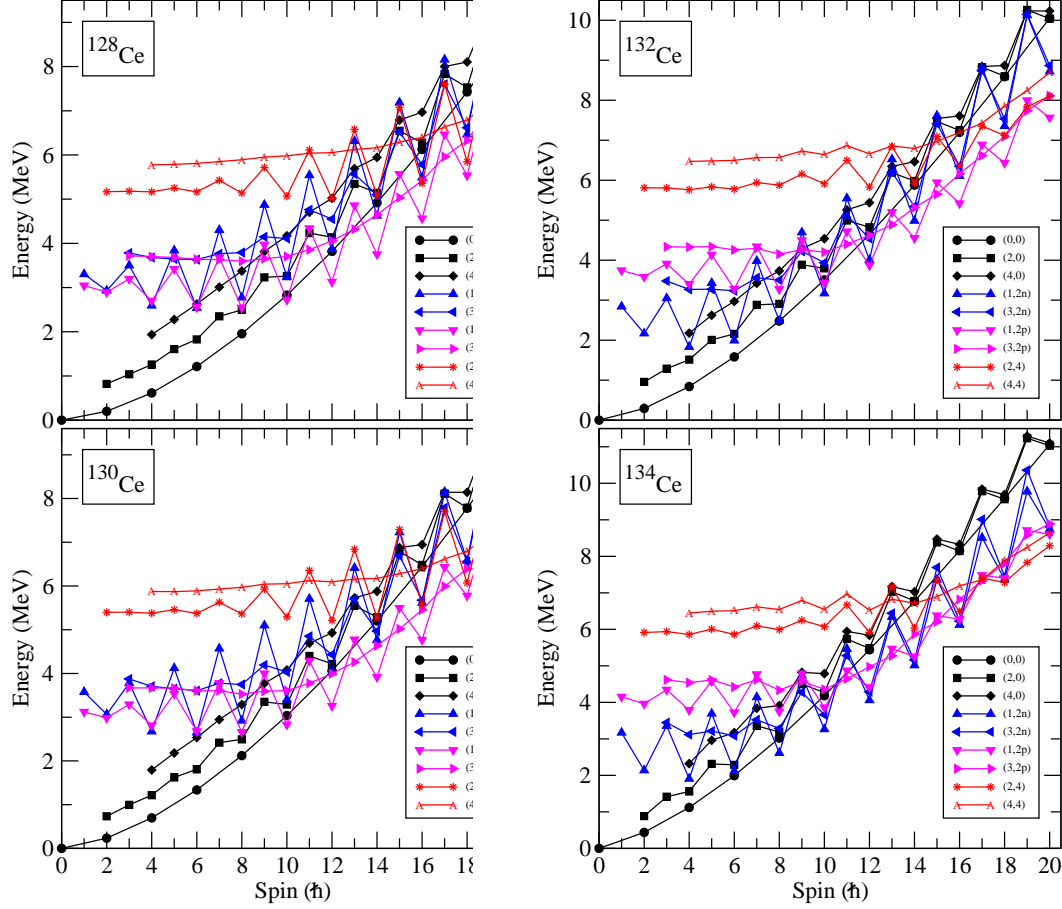


Fig. 3. (Color online) Band diagrams for $^{128-134}\text{Ce}$ isotopes.

that the $2n$ state $(1, 2n)$ and $2p$ state $(1, 2p)$ become yrast at the same angular momentum of $I = 10$ with the neutron band slightly lower than the proton band. However, for higher angular momenta, the proton band is observed to be favored in energy, and is yrast up to the highest spin value. For ^{134}Ce , the neutron-aligned band $(1, 2n)$ crosses the ground band $(0, 0)$ at $I = 8$, and this band is yrast up to $I = 16$. Above this spin value, it is noted that the 4-qp band $(2, 4)$ with both protons and neutrons aligned becomes favored.

Band diagrams of the Nd isotopes are shown in Fig. 4. It is seen that the $(2, 0)$ and $(4, 0)$ bandheads are, respectively, at 1 and 2 MeV excitation energy in ^{132}Nd . The $2p$ aligned bandhead is lower in energy than the $2n$ band with the result that the proton band $(1, 2p)$ crosses the ground band $(0, 0)$ at $I = 12$, and becomes yrast for all the spin values above it. For ^{134}Nd , the $2n$ bandhead is now lower in energy than the $2p$ one, and at $I = 10$ both these aligned bands cross the ground band and it is, therefore expected that this nucleus should depict forking of the ground state band into two s-bands. Above the band-crossing region in ^{134}Nd , the yrast even- I states originate from the $(1, 2p)$ and the odd- I states arise from the $(3, 2p)$ band. The lowest two bands above $I = 12$ originate from the same $2p$ states and, therefore, will have positive

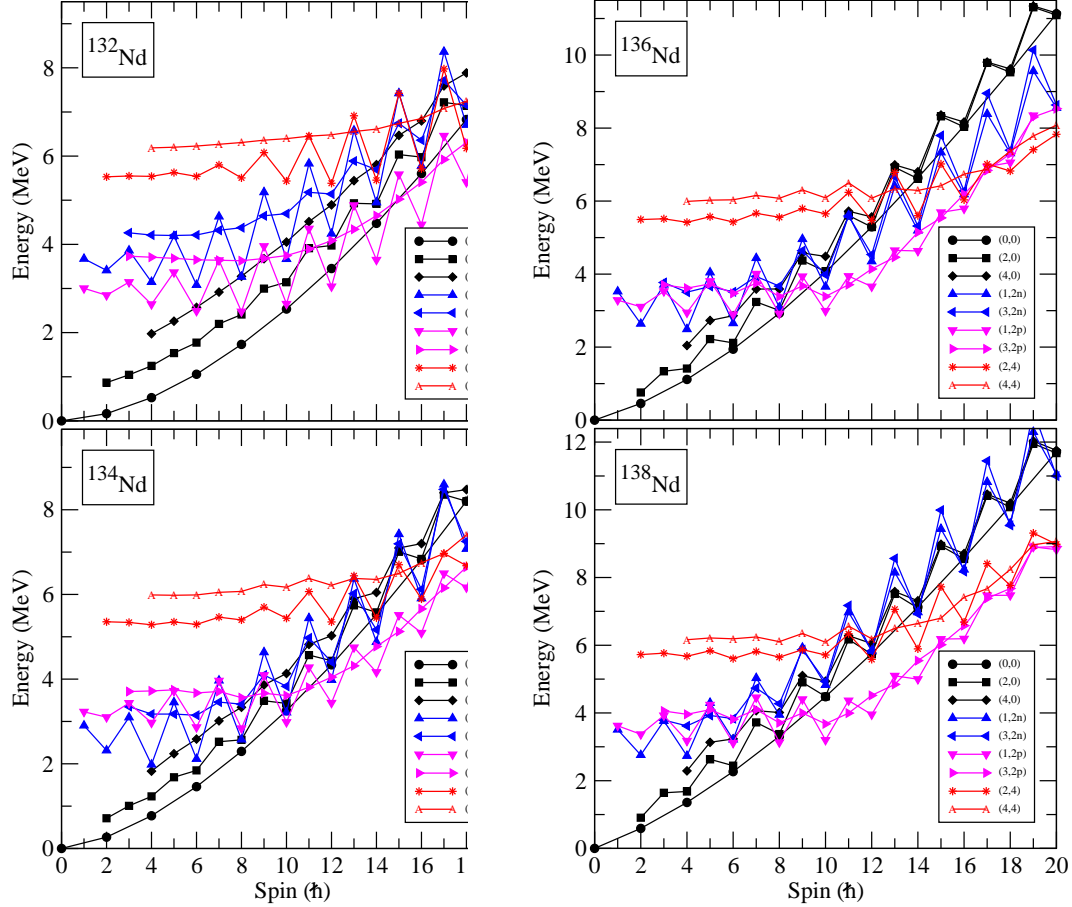


Fig. 4. (Color online) Band diagrams for $^{132-138}\text{Nd}$ isotopes.

g-factors, opposite to that of the ^{134}Ce case.

For $^{136,138}\text{Nd}$ in Fig. 4, the γ -bands are very close to the yrast line. In ^{136}Nd , the band-crossing occurs at $I = 8$, and for ^{138}Nd it is at $I = 10$. In both nuclei, proton- and neutron-aligned bands cross the ground band and, therefore, it is expected that both nuclei should show forking of the ground state band into two s-bands. Further, it is noted that in ^{138}Nd the $(3, 2p)$ band is also very low in energy and is the first excited band above $I = 10$ for even-spin states. For odd-spin states, it forms the yrast band.

In the mass region under investigation, there have been observations of high-spin states at low excitation energies. We previously mentioned ^{134}Ce as a particular example where two lowest 10^+ states were detected at excitation energy 3.2086 MeV and 3.7193 MeV, respectively. In Fig. 5, we collect all the experimentally known 10^+ states for nuclei studied in this paper. At first glance, these could be bandheads of some multi-qp bands associated with high- K configurations. However, a close look indicates that there are no such high- K configurations available around the Fermi surfaces. From our band diagrams shown in Figs. 3 and 4, we see that in nuclei with $N = 76$ and 78 ,

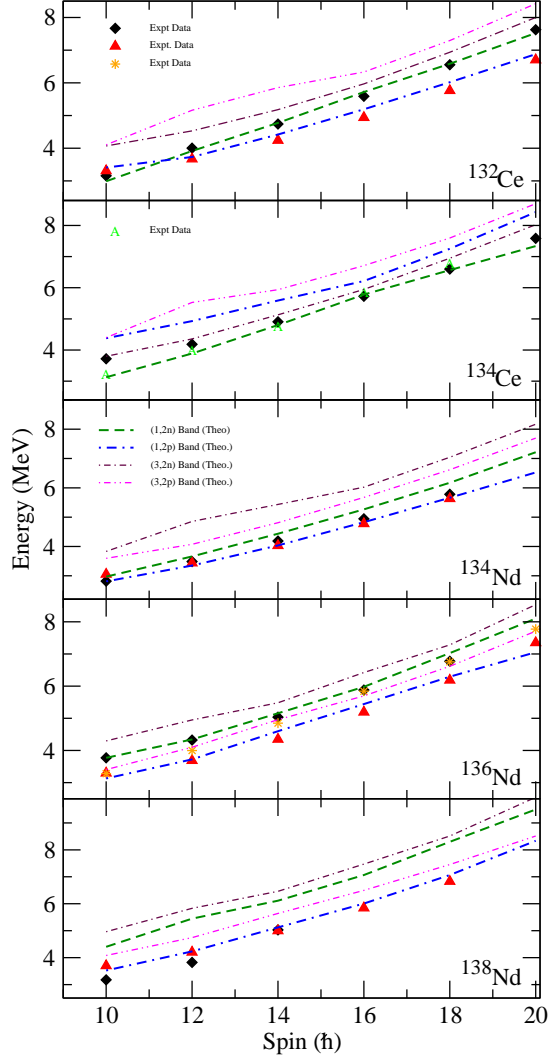


Fig. 5. (Color online) Four theoretical bands with the main component from $(1, 2n)$, $(1, 2p)$, $(3, 2n)$, and $(3, 2p)$, respectively. Only the spin range from $I = 10$ to 20 is shown in which these bands are low in energy. Available data in $^{132,134}\text{Ce}$ and $^{134,136,138}\text{Nd}$ are compared with the calculation.

more than one band crosses the ground band at $I = 10$. The crossing bands are not high- K bands, but bands having low- K configurations.

The two $I = 10^+$ states in ^{134}Ce were long ago identified experimentally. However, the structure of these 10^+ states remained a puzzle. The magnetic moment of both states has been measured, and it has been found that both have negative g -factors [12]. This suggests that both the 10^+ states have a neutron structure. This was a surprising finding because normally two lowest-lying 2-qp states should separately belong to 2-quasineutron and 2-quasiproton states. In ref. [30], an explanation was proposed. Now looking at our Fig. 3, one can easily see that in ^{134}Ce , apart from the $2n$ band $(1, 2n)$ and the $2p$ band $(1, 2p)$, the γ -band built on the $2n$ band $(3, 2n)$ also crosses the ground

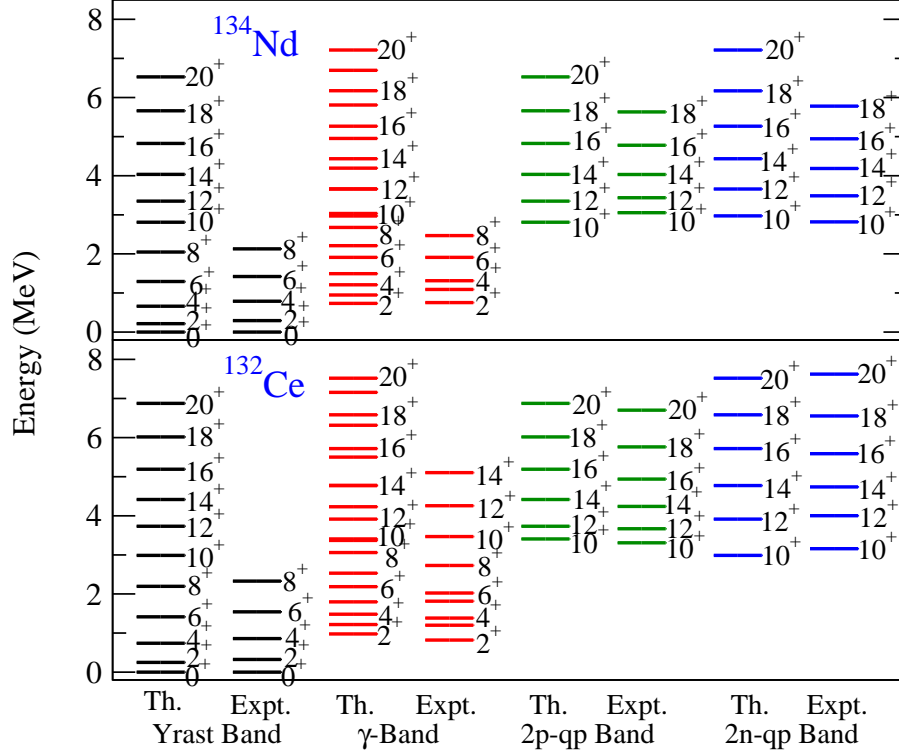


Fig. 6. (Color online) Level schemes for ^{132}Ce and ^{134}Nd . Comparison between the calculated levels and experimental data is made for four bands: the yrast bands, the γ bands, and the $I = 10^+$ 2-qp bands based on γ vibration.

band (0, 0) at $I = 10$. Thus at $I = 10$, there are at least three states below that of the ground band, which are (from lower to higher energies) $(1, 2n)$, $(3, 2n)$, and $(1, 2p)$. It is very interesting that for this nucleus, the neutron 2-qp band based on γ -vibration $(3, 2n)$ is predicted to appear lower in energy than the proton 2-qp band $(1, 2p)$. Therefore, the lowest two $I = 10^+$ states, one being a 2-qp state built on the ground state and the other a 2-qp state on the γ -vibration, have both neutron configuration. This is consistent with the g-factor measurement [12], and thus naturally explains the structure of the two 10^+ bands.

Fig. 5 summarizes the results regarding the theoretical γ - bands built on 2-qp states obtained after diagonalization of the shell-model Hamiltonian. The calculated bands associated with the four most relevant and dominant states are displayed: (1) $(1, 2n)$, the 2-qp neutron $K = 1$ state built on the qp vacuum state; (2) $(1, 2p)$, the 2-qp proton $K = 1$ state on the vacuum state; (3) $(3, 2n)$, the 2-qp neutron $K = 3$ state on the collective γ -vibration; and (4) $(3, 2p)$, the 2-qp proton $K = 3$ state on the γ -vibration. Only even spin members (energetically favored) of each band are shown and compared with available data. It is quite interesting to note that the relative position of the four bands varies in each nucleus. We have discussed the case of ^{134}Ce where the lowest two are both neutron states. From Fig. 5, our calculation further predicts that

in $^{136,138}\text{Nd}$, one may observe two lowest $I = 10^+$ states but with a proton structure. The g-factor measurement in these two nuclei is expected to lead to large, positive values, in sharp contrast to those in ^{134}Ce .

Finally, in order to depict the comparison between the experimental and theoretical energies more clearly, we plot in Fig. 6 the calculated and experimental level energies for the yrast bands, the γ bands, and the $I = 10^+$ 2-qp bands based on γ vibration. We have chosen two nuclei, ^{132}Ce and ^{134}Nd , as examples and the results are similar for other studied nuclei. It is quite evident from this figure that not only the levels within each band, but also the relative positions of the bands, are reasonably well reproduced by the TPSM approach.

4 Summary

The results presented in this work suggest that multi-qp states in a triaxially deformed well can exhibit much more fruitful band structures. This is because with triaxiality, a single configuration contains a rich mixture of many possible K -states and after angular momentum projection, each one of them corresponds to a rotational band. It was pointed out in ref. [14] that the projected triaxial vacuum state alone can already produce the collective ground state band, γ -band, 2γ -band, etc. Similarly, a projected 2-qp state can give rise to 2-qp bands with $K = 1, 3, 5, \dots$. If the $K = 1$ band is a 2-qp band based on the ground state, then the $K = 3$ band can be understood as a 2-qp band based on the γ -vibration, and the $K = 5$ band as a 2-qp band based on the 2γ state, etc. This pattern can be clearly seen when multi-qp configurations constructed from a triaxially deformed well are projected on good angular momentum. The picture thus extends the simple surface γ oscillation in deformed nuclei where paired nucleons vibrate coherently in the deformed vacuum state.

Summarizing the present work, multi-qp band structures in some neutron-deficient Ce and Nd isotopes has been studied using the extended triaxial projected shell-model approach. It has been demonstrated that γ -band built on the 2-qp configurations can modify the band-crossing features in these nuclei. The 2-qp γ -band with $K = 3$ are shown to be energetically favored for some angular-momentum states and form the first excited bands in nuclei studied in the present work. For ^{134}Ce , it is shown that the lowest two $I = 10^+$ states originate from the same 2-quasineutron configuration and sheds new light on the observation of negative g-factors for the two states. Further, it is predicted that the lowest two $I = 10^+$ states in $^{136,138}\text{Nd}$ originate from the same $2p$ configuration and both these states should have positive g-factors. The present results have enriched the concept of γ -vibration and we hope that, in the future, more states of such kind will be identified experimentally.

5 Acknowledgments

Research at ORNL is supported by the Division of Nuclear Physics, U.S. Department of Energy, under Contract DE-AC05-00OR22725 with UT-Battelle, LLC. Research at SJTU is supported by the National Natural Science Foundation of China under contract No. 10875077 and by the Chinese Major State Basic Research Development Program through grant 2007CB815005.

References

- [1] E. S. Paul *et al.*, Phys Rev. C **71** (2005) 054309.
- [2] P. Mason *et al.*, Phys. Rev. C **72** (2005) 064315.
- [3] C. M. Petrache *et al.*, Phys. Lett. **387 B** (1996) 31.
- [4] S. Lakshmi *et al.*, Nucl. Phys. **A 761** (2005) 1.
- [5] S. Sihotra *et al.*, Phys. Rev. C **78** (2008) 034313.
- [6] A. Gade *et al.*, Nucl. Phys. **A 673** (2000) 45.
- [7] W. F. Mueller *et al.*, Phys. Rev. C **73** (2006) 014316.
- [8] A. Jungclaus *et al.*, Phys. Rev. C **77** (2008) 024310.
- [9] T.R. Saito, *et al.*, Phys. Lett. **B 669** (2008) 19.
- [10] R. Wyss, J. Nyberg, A. Johnson, R. Bengtsson and W. Nazarewicz, Phys. Lett. **B 215** (1988) 211.
- [11] W. Satula and R. Wyss, Physica Scripta **T 56** (1995) 159.
- [12] A. Zemel *et al.*, Nucl. Phys. **A 383** (1982) 165.
- [13] J. A. Sheikh and K. Hara, Phys. Rev. Lett. **82** (1999) 3968.
- [14] Y. Sun, K. Hara, J. A. Sheikh, J. G. Hirsch, V. Velazquez, M. Guidry, Phys. Rev. C **61** (2000) 064323.
- [15] J. A. Sheikh, G. H. Bhat, Y. Sun, G. B. Vakil, R. Palit, Phys Rev. C **77** (2008) 034313.
- [16] Z.-C. Gao, Y.-S. Chen, Y. Sun, Phys. Lett. **B 634** (2006) 195.
- [17] K. Hara and Y. Sun, Int. J. Mod. Phys. **E4** (1995) 637.
- [18] M. Dufour and A. P. Zuker, Phys. Rev. C **54** (1996) 1641.
- [19] M. Hasegawa and K. Kaneko, Phys. Rev. C **59** (1999) 1449.

- [20] S. G. Nilsson *et. al.*, Nucl. Phys. **A 131** (1969) 1.
- [21] P. Möller and J. R. Nix, At. Data Nucl. Data Tables **59** (1995) 185.
- [22] We thank H.-L. Liu for the TRS calculation with the method discribed by F. R. Xu, P. M. Walker, R. Wyss, Phys. Rev. C **65** (2002) 021303(R).
- [23] E. S. Paul *et. al.*, Nucl. Phys. **A 676** (2000) 32.
- [24] B. Singh, Nucl. Data Sheets **93** (2001) 33.
- [25] A. A. Sonzogni, Nucl. Data Sheets **103** (2004) 1.
- [26] Yu. Khazov *et al.*, Nucl. Data Sheets **104** (2005) 497.
- [27] C. M. Petrache *et. al.*, Phys. lett. **B 387** (1996) 31.
- [28] O. Zeidan *et. al.*, Phys. Rev. C **66** (2002) 044311.
- [29] E. Mergel *et. al.*, Eur. Phys. J. **A 15** (2002) 417.
- [30] R. Wyss *et. al.*, Nucl. Phys. **A 505** (1989) 337.